PHYSICAL REVIEW B **93**, 161115(R) (2016)

Scanning Josephson spectroscopy on the atomic scale

Mallika T. Randeria,* Benjamin E. Feldman,* Ilya K. Drozdov,† and Ali Yazdani‡
Joseph Henry Laboratories and Department of Physics, Princeton University, Princeton, New Jersey 08544, USA
(Received 11 January 2016; revised manuscript received 11 April 2016; published 28 April 2016)

The Josephson effect provides a direct method to probe the strength of the pairing interaction in superconductors. By measuring the phase fluctuating Josephson current between a superconducting tip of a scanning tunneling microscope and a BCS superconductor with isolated magnetic adatoms on its surface, we demonstrate that the spatial variation of the pairing order parameter can be characterized on the atomic scale. This system provides an example where the local pairing potential suppression is not directly reflected in the spectra measured via quasiparticle tunneling. Spectroscopy with such superconducting tips also shows signatures of previously unexplored Andreev processes through individual impurity-bound Shiba states. The atomic resolution achieved here establishes scanning Josephson spectroscopy as a promising technique for the study of novel superconducting phases.

DOI: 10.1103/PhysRevB.93.161115

A number of novel superconducting states of matter such as those appearing in disordered superconductors, heavy fermion materials, and high-T_c superconductors have been predicted to have pairing order parameters that are spatially modulated on atomic length scales. These short range spatial modulations can occur due to different mechanisms such as the inhomogeneous material properties in disordered superconductors [1–4], a momentum dependent pairing interaction, such as the Fulde-Ferrell-Larkin-Ovchinnikov state proposed for heavy fermion materials [5–7], or the interplay between different forms of electronic ordering in the pair density waves proposed for high-T_c cuprates [8–10]. Although spectroscopic mapping with a scanning tunneling microscope (STM) can provide evidence for variations in the local density of states (LDOS) through quasiparticle tunneling, such measurements probe the superconducting order parameter only indirectly. If the Josephson effect can be measured and mapped on the atomic scale, then it would allow for direct characterization of the local pairing order parameter and high-resolution studies of novel superconducting phases [11].

This goal has motivated previous efforts in the use of superconducting tips in STMs [12] and has led to the local observation of thermal phase fluctuating Josephson supercurrent close to the point contact regime [13–15]. Subsequent measurements have mapped the Josephson effect on the nanometer scale, applying this technique to vortices [16,17] and high-T_c cuprates [18,19]. A major challenge in improving the resolution of these experiments has been satisfying the competing requirements of a high junction impedance necessary for imaging and a low junction impedance allowing for the strong tip-sample coupling necessary to observe the Josephson effect despite thermal fluctuations. Extending the Josephson STM measurements to millikelvin temperatures allows for mapping of the Cooper pair current at junction resistances that are compatible with atomic resolution imaging.

Here, we use scanning Josephson spectroscopy to probe variations of the superconducting order parameter on the scale of a single atom. We map the strength of the phase fluctuating Josephson current between a superconducting Pb tip and a Pb(110) surface with a dilute concentration of magnetic impurities using a dilution refrigerator STM system. By modeling the interaction of the electromagnetic environment with our Josephson STM setup, we can understand the spectroscopic data taken with a superconducting tip, including the signatures of photon-assisted inelastic Cooper pair tunneling at nonzero bias. Our measurements show a 10%–15% reduction of the Josephson critical current I_c over a few angstrom length scale in the vicinity of the magnetic adatoms, thereby demonstrating a local suppression of the order parameter. We do not observe a commensurate shift in the coherence peak energies in the single particle spectrum, which is consistent with theoretical calculations [20,21], highlighting the ability of the Josephson STM technique to probe physics inaccessible through traditional STM quasiparticle tunneling. Additionally, spatially resolved spectroscopy with a superconducting tip allows us to detect novel Andreev tunneling processes through impurity-bound Shiba states of the individual adatoms.

Our measurements have been carried out using a home built dilution refrigerator STM system, with a base temperature of 20 mK and a spectroscopic resolution that corresponds to an effective electron temperature of 250 mK [22]. For the present experiments, we used a Pb(110) single crystal that was prepared *in situ* with several cycles of Ar sputtering and annealing to produce an atomically ordered flat surface. Figure 1(a) shows differential conductance dI/dV measurements of the atomic Pb(110) surface [inset of Fig. 1(a)] measured using a normal W tip at base temperature. The two coherence peaks in the spectrum are indicative of two pairing gaps in bulk Pb associated with two different Fermi surfaces. As shown in this figure, the data can be modeled using a sum of two BCS densities of states with corresponding gaps, $\Delta_1 = 1.26$ meV and $\Delta_2 = 1.42$ meV, including an energy broadening associated with finite temperature (250 mK) and a quasiparticle lifetime (8 μeV). Although the two gaps in Pb have been previously detected in planar junctions [23,24] and in STM studies using superconducting tips [25], our ability to resolve them with a

*These authors contributed equally to this work.
†Present address: Brookhaven National Laboratory, Upton, NY 11973.
‡yazdani@princeton.edu

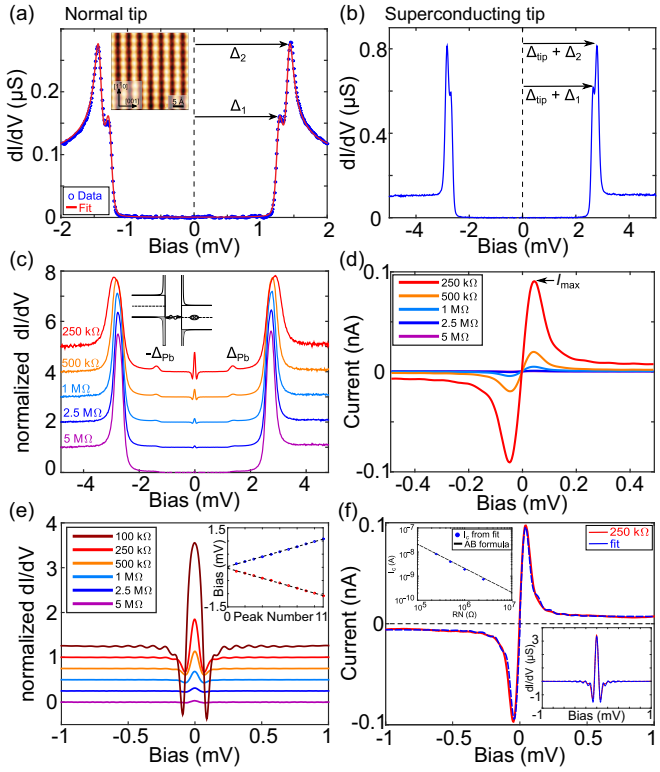

FIG. 1. (a) dI/dV of Pb(110) with a normal tip resolving two superconducting gaps. Inset: Atomic scale topography of the Pb(110) surface. (b) dI/dV of Pb(110) with a superconducting Pb tip. (c) Superconducting tip spectroscopy on Pb(110), normalized to R_N. Curves are offset for clarity. As junction resistance is decreased, features due to Andreev reflections ($eV = \pm\Delta_{\rm Pb}$) and the Josepshon effect ($V = 0$) become more pronounced. Due to the quality of the tip, the two superconducting gaps of Pb are not clearly resolved. Inset: Schematic of an Andreev process between two superconductors with the same gap, occurring at a threshold $e|V| = \Delta_{\rm Pb}$. (d) IV characteristics of the STM Josephson junction around zero bias, for different normal state resistance R_N. (e) Oscillations in dI/dV (offset for clarity, normalized to R_N) due to photon-assisted Cooper pair tunneling with characteristic frequency of $\nu_0 \approx 23$ GHz, determined by fitting the bias of the peaks as a function of oscillation number (inset). (f) Fit to IV and dI/dV (bottom right inset) data for $R_N = 250$ kΩ using the $P(E)$ theory. Top left inset: Values of critical current extracted from $P(E)$ fits (blue dots), in agreement with the Ambegaokar-Baratoff formula (black). All point spectra in this figure were acquired at a parking bias of $V = -5$ mV at which the normal state junction resistance was determined (well outside the superconducting gap).

normal tip demonstrates the high energy resolution afforded by the low temperature operation of our system.

To create a Josephson junction in our STM setup, we prepare a superconducting Pb tip by indenting a W tip into the Pb(110) substrate until the spectra measured with such a tip exhibit features indicative of quasiparticle tunneling between two superconductors [12,25]. As seen in Fig. 1(b), the tunneling spectra with such tips show sharp coherence peaks at voltages corresponding to the sum of the tip and substrate superconducting gaps, with a tip gap $\Delta_{\rm tip}$ ranging from 1.3 to 1.4 meV (approximately that of bulk Pb), depending on the tip. We do not resolve additional structure in the coherence peaks arising from multiple gaps in the tip, which suggests that the superconducting apex of the tip is amorphous in nature, consistent with previous measurements [25]. For simplicity, we assume below that the gap of the tip and sample are the same and define $\Delta_{\rm Pb} \simeq (\Delta_1 + \Delta_2)/2 \simeq \Delta_{\rm tip} \approx 1.35$ meV.

While spectroscopy at high junction resistances with the Pb tips show only signatures of quasiparticle tunneling, even at junction resistances of about 2.5 MΩ, we begin to resolve features associated with Andreev reflections and Cooper pair tunneling between the tip and the sample [Fig. 1(c)]. Successively decreasing the junction impedance highlights the evolution of distinct features at the characteristic energy of $\pm\Delta_{\rm Pb}$, arising from Andreev processes in the STM junction [26] as illustrated in the inset of Fig. 1(c). The prominent peak in conductance at zero bias corresponds to the IV characteristic shown in Fig. 1(d), where the maximum Cooper pair current $I_{\rm max}$ occurs at a voltage near zero bias ($V_p \approx 40\ \mu$V) due to a phase fluctuating Josephson supercurrent, discussed in more detail below. Moreover, we resolve periodic features in both current and conductance that appear at remarkably regular voltage intervals (95 μV), which are related to the interaction of the STM Josephson junction with its electromagnetic environment [Fig. 1(e)]. Finally, we also note that at low junction impedances, the large injection of quasiparticles results in an increased broadening of the coherence peaks compared to spectra at higher junction resistance [Fig. 1(c)].

We can understand the spectroscopic features of our STM Josephson junction by comparing the magnitude of the three relevant energy scales: (i) the Josephson coupling energy between the tip and sample, $E_J = \pi\hbar/(4e^2)\cdot(\Delta_{\rm Pb}/R_N) = \hbar/(2e)\cdot I_c$, which depends on the normal state junction resistance R_N and the pairing gap $\Delta_{\rm Pb}$; (ii) the thermal energy corresponding to the electron temperature, $k_BT = 22\ \mu$eV; and (iii) the charging energy $E_C = (2e)^2/2C$, which depends on the capacitance C of the junction. For our STM junction with a typical $C \approx 4$ fF, most measurements are performed in a regime where the charging energy dominates the behavior of the Josephson junction, $E_J \lesssim k_BT \ll E_C$. In this case, the thermal fluctuations of the phase across the junction are enhanced by quantum fluctuations, which together result in a shift of the Josephson pair current to nonzero bias [27], as we observe in the data shown in Fig. 1(d). The oscillations in the conductance at higher bias [Fig. 1(e)] arise from the interaction between such a phase incoherent Josephson junction and the standing electromagnetic modes associated with the STM tip. Photon absorption or emission with energy $E = h\nu = 2eV$ facilitates Cooper pair tunneling across the STM junction at nonzero bias, a signature similar to the ac Josephson effect [28,29]. Treating the STM setup as an open-ended $\lambda/4$ antenna with resonances at $\nu_n = (2n+1)\cdot c/l$ [28] allows us to fit the voltage spacing of the oscillations to extract a characteristic frequency $\nu_0 \approx 23$ GHz, which is intrinsic to our instrument, corresponding to an approximate tip length $l = 3.3$ mm. The high quality factor of these oscillations highlights the sensitivity of the STM Josephson junction to its electromagnetic environment.

A quantitative understanding of our Josephson STM characteristics can be obtained by using the $P(E)$ theory to model

the probability of Cooper pair tunneling across the junction mediated by its electromagnetic environment [27,30]. The energy exchange with the environment as well as thermal effects contribute to inelastic pair tunneling across the junction. As shown in the fit in Fig. 1(f), we can accurately capture the particular shape of our spectra using this theory, the details of which are discussed in the Supplemental Material [31]. Within this model, both the maximal phase-fluctuating pair current $I_{\max}$ and the differential conductance at zero bias are proportional to the square of the intrinsic Josephson critical current, I_c^2 [27,30,32]. The values that we obtain for the intrinsic I_c as a function of the normal state junction resistance R_N are in good agreement with calculations from the Ambegaokar-Baratoff formula, $I_c = \pi/(2e) \cdot \Delta_{\mathrm{Pb}}/R_N$ [33], as shown in the top inset of Fig. 1(f), justifying the use of this model to fit the data. Although the small capacitance of a typical STM junction makes such Josephson junctions phase incoherent, mapping of the phase-fluctuating pair current at low bias in the STM setup still provides a direct method for the spatial characterization of the pairing amplitude in a superconducting sample.

To demonstrate that the Josephson STM technique can probe variations of the order parameter on the atomic scale, we investigate individual magnetic atoms deposited on the surface of the Pb(110) substrate. Magnetic impurities on an *s*-wave superconductor are the simplest example of pair-breaking defects that are well known to suppress superconductivity, for instance seen in the suppression of T_c with increasing impurity concentration [34,35]. Previous STM spectroscopy has used quasiparticle tunneling to show that magnetic atoms on a BCS superconductor induce in-gap Shiba states [36–41]; however, such LDOS measurements do not directly probe the superconducting order parameter. To probe the spatial variation of the pairing strength for this model system, we deposit a submonolayer of Fe adatoms on Pb(110) *in situ*, at a temperature of about 20 K. As shown in a typical STM topography [Fig. 2(a)], this low temperature deposition results in the appearance of features with angstrom height, which are consistent with individual Fe atoms residing in two different atomic sublattice binding sites (types *A* and *B*) on the Pb(110) substrate [Figs. 2(d) and 2(h)].

To probe the pairing amplitude near these magnetic Fe atoms, we perform spectroscopic measurements using superconducting Pb tips at junction resistances that are low enough to detect the phase-fluctuating Josephson current but high enough to perform STM imaging without disrupting the adatoms on the surface. As shown in Figs. 2(b) and 2(f), IV measurements of the two different types of Fe adatom sites show a suppression of the peak in the pair current $I_{\max}$ near zero bias as compared to the bare substrate, also seen in an analogous measurement of differential conductance over the magnetic impurities [Figs. 2(c) and 2(g)]. This reduction of the phase-fluctuating pair current and conductance is a direct signature of the local suppression of the pairing amplitude caused by the magnetic impurities, corresponding to a 10%–15% reduction of the critical current I_c on an Fe adatom based on fits to the spectra (see Supplemental Material). The precise value of $I_{\max}$ and the zero-bias conductance depend on the superconducting tips and the strength of the exchange coupling between the impurity and underlying Pb substrate (as is evident from the difference between type-*A* and type-*B* adatoms), but the suppression of the intrinsic critical current is consistent across dozens of adatoms measured with various different Pb tips.

Another measurement that reflects the local pairing suppression is mapping the differential conductance at zero bias in the vicinity of the Fe defects to probe the spatial variations of the order parameter. These measurements, shown in Figs. 2(e) and 2(i), demonstrate our key finding that this Josephson STM technique can resolve spatial variations of the pairing amplitude on the atomic scale. Data from additional adatoms showing a suppression of the order parameter, as

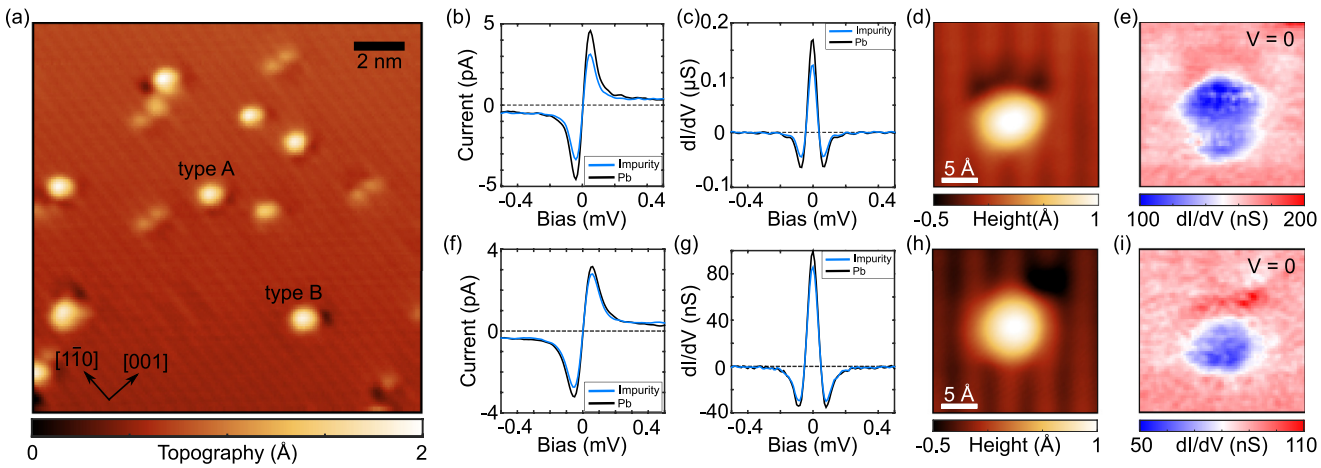

FIG. 2. (a) Topography of Pb after evaporating a submonolayer of Fe. Individual Fe adatoms tend to be centered on a trench (type *A*) or row (type *B*) of the Pb(110) surface as marked. Suppression of pair current [(b),(f)] and dI/dV [(c),(g)] on the Fe adatom (blue) compared to on Pb (black) at 1 MΩ junction impedance for type *A* [(b)–(e)] and type *B* [(f)–(i)] adatoms. Simultaneous topographies [(d),(h)] and differential conductance maps [(e),(i)] at $V = 0$ for $R_N = 1$ MΩ demonstrate the spatial suppression of the Josephson effect over the Fe adatoms. Parking conditions $V = -5$ mV and $I = 5$ nA for data in (b)–(i), ensuring that R_N is the same over both the adatom and bare Pb. Different superconducting tips were used for the point spectra and the conductance maps, but the I_c suppression is consistent across measurements.

well as control experiments that rule out artifacts of tip height variations are detailed in the Supplemental Material.

Our observation that the pairing amplitude recovers back to its unperturbed value for the Pb within angstroms of the magnetic adatoms, and not on the scale of the coherence length is consistent with theoretical predictions [42,43]. Theory also predicts an oscillating power law for the order parameter, $\Delta(r) \sim \sin^2(k_F r)/(k_F r)^2$ as a function of the distance r from a magnetic impurity, where k_F is the Fermi wave vector [43]. However, both the adatom geometry on the surface of a three-dimensional superconductor and the short Fermi wavelength in Pb give rise to the short-range decay of the order parameter, making it difficult to detect these oscillations in the current experiment.

In contrast, the suppression of the local order parameter is not prominently seen in quasiparticle tunneling measurements over the magnetic impurity. Superconducting tip spectra [Fig. 3(a)] over an Fe adatom show a suppression in the intensity of the coherence peaks with no appreciable shift in their energy as compared to the bare substrate. In the presence of bound states, the spectral weight is redistributed from the coherence peaks to the bound state energies and the suppression of the local pairing amplitude does not translate into a shift in the energies of the coherence peaks.

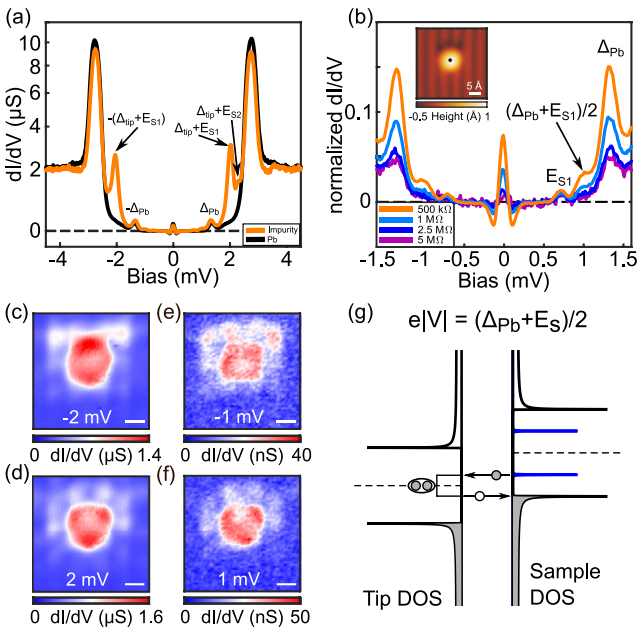

FIG. 3. (a) dI/dV with a superconducting tip ($V = -5$ mV, $I = 10$ nA) on a type A impurity, plotted on a log scale, showing the appearance of Shiba states at $\Delta_{\rm Pb} + E_{S1} = \pm 2.06$ meV and $\Delta_{\rm Pb} + E_{S2} = +2.28$ meV (marked by arrows). (b) A zoom-in of dI/dV at lower junction resistances highlights multiple Andreev reflections through the Shiba state observed at energies $\pm(\Delta_{\rm Pb} + E_{S1})/2$. Parking bias $V = -5$ mV for all spectra. [(c)-(f)] Conductance maps at $eV = \pm(\Delta_{\rm Pb} + E_{S1})$ and $eV = \pm(\Delta_{\rm Pb} + E_{S1})/2$ taken simultaneously with the topograph in the inset of (b). Corresponding spatial patterns between the Shiba state ($V = 2$ mV) and the Andreev reflection state ($V = 1$ mV), and similarly for states at negative bias are observed. Scale bar is 5 Å. (g) Schematic for the Andreev reflection process with threshold voltage $eV = \pm(\Delta_{\rm Pb} + E_{S1})/2$, where the relevant energy gap is that of the sample.

Self-consistent calculations confirm this distinction between measurements of the order parameter and the local density of states [20,21]. Thus, our measurements demonstrate the utility of scanning Josephson spectroscopy in directly extracting local variations of the superconducting order parameter.

Spectroscopic measurements with a superconducting tip can also be used to probe previously unexplored Andreev reflection processes through the in-gap Shiba states localized near individual magnetic adatoms. Typically, impurity-bound Shiba states are detected in measurements with superconducting tips through quasiparticle or Andreev tunneling processes at energies of $e|V| = \Delta_{\rm tip} + E_S$, where E_S is the energy of the Shiba state [40,44]. Performing similar measurements on the Fe defects, we observe the expected signatures of the Shiba states, an example of which is shown in Fig. 3(a) for a type-A Fe defect. We resolve two different Shiba states at $e|V| = \Delta_{\rm tip} + E_{S1}$ and $eV = \Delta_{\rm tip} + E_{S2}$. Examining the dependence of such measurements on the coupling between the superconducting tip and sample, we find that at lower junction resistance, there are additional subgap features in the spectra at lower biases [Fig. 3(b)]. In particular, peaks occur in conductance at $e|V| = (\Delta_{\rm Pb} + E_{S1})/2$, which correspond to previously undetected Andreev reflections through an impurity-bound Shiba state. We also resolve peaks at $e|V| = E_{S1}$, which arises at least in part from direct quasiparticle tunneling from an imperfect superconducting tip (see Supplemental Material). The feature at $e|V| = (\Delta_{\rm Pb} + E_{S1})/2$, which is due to a subgap tunneling process, cannot occur due to quasiparticle tunneling but rather arises from an Andreev process through the Shiba state, as illustrated in Fig. 3(g). Further corroboration that such Andreev processes involve the localized Shiba state can be obtained by comparing the spatial patterns of maps over the impurities at the Andreev reflection energy $[e|V| = (\Delta_{\rm Pb} + E_{S1})/2]$ with that of tunneling at $e|V| = \Delta_{\rm Pb} + E_{S1}$. The excellent correspondence between the holelike (electronlike) conductance measurements shown in Figs. 3(c) and 3(e) [Figs. 3(d) and 3(f)] for the type-A impurity demonstrates the role of Shiba states in such Andreev processes. The Supplemental Material includes other examples and a discussion of possible complications due to imperfect tips.

In conclusion, we demonstrate that combining Josephson spectroscopy with atomic resolution STM imaging provides a method to directly probe the local superconducting order parameter, which is not directly accessible through traditional quasiparticle measurements. Despite the challenge of operating such Josephson junctions in a fully phase coherent regime due to their ultrasmall dimensions, the fluctuating pair current is still a powerful tool to examine spatial variations of the pairing amplitude. Our key accomplishment, demonstrating that these measurements can be performed with atomic resolution, paves the way for using scanning Josephson techniques to study an inhomogeneous or spatially modulated order parameter in novel superconducting materials.

We would like to thank J. Li, B. Jäck, and F. Pientka for valuable discussions. This work has been supported by the Gordon and Betty Moore Foundation as part of EPiQS

initiative (GBMF4530) and DOE-BES. This project was also made possible using the facilities at Princeton Nanoscale Microscopy Laboratory supported by Grants No. NSF-DMR-1104612, No. ARO-W911NF-1-0262, No. ONR-N00014-14-1-0330, No. ONR-N00014-13-10661, DARPA-SPWAR Meso program N6601-11-1-4110, LPS and ARO-W911NF-1-0606, and NSF-MRSEC programs through the Princeton Center for Complex Materials DMR-1420541. M.T.R. acknowledges support from the NSF Graduate Research Fellowship Program.

[1] B. Sacepe, T. Dubouchet, C. Chapelier, M. Sanquer, M. Ovadia, D. Shahar, M. Feigel'man, and L. Ioffe, Nat. Phys. **7**, 239 (2011).
[2] K. Bouadim, Y. L. Loh, M. Randeria, and N. Trivedi, Nat. Phys. **7**, 884 (2011).
[3] K. K. Gomes, A. N. Pasupathy, A. Pushp, S. Ono, Y. Ando, and A. Yazdani, Nature (London) **447**, 569 (2007).
[4] A. N. Pasupathy, A. Pushp, K. K. Gomes, C. V. Parker, J. Wen, Z. Xu, G. Gu, S. Ono, Y. Ando, and A. Yazdani, Science **320**, 196 (2008).
[5] P. Fulde and R. A. Ferrell, Phys. Rev. **135**, A550 (1964).
[6] A. J. Larkin and Yu. N. Ovchinnikov, Zh. Eksp. Teor. Fiz. **47**, 1136 (1964) [Sov. Phys. JETP **20**, 762 (1965)].
[7] Y. Matsuda and H. Shimahara, J. Phys. Soc. Jpn. **76**, 051005 (2007).
[8] H.-D. Chen, O. Vafek, A. Yazdani, and S.-C. Zhang, Phys. Rev. Lett. **93**, 187002 (2004).
[9] E. Berg, E. Fradkin, and S. A. Kivelson, Nat. Phys. **5**, 830 (2009).
[10] P. A. Lee, Phys. Rev. X **4**, 031017 (2014).
[11] J. Šmakov, I. Martin, and A. V. Balatsky, Phys. Rev. B **64**, 212506 (2001).
[12] J. Rodrigo and S. Vieira, Phys. C (Amsterdam, Neth.) **404**, 306 (2004).
[13] O. Naaman, W. Teizer, and R. C. Dynes, Phys. Rev. Lett. **87**, 097004 (2001).
[14] J. G. Rodrigo, H. Suderow, and S. Vieira, Eur. Phys. J. B **40**, 483 (2004).
[15] N. Levy, T. Zhang, J. Ha, F. Sharifi, A. A. Talin, Y. Kuk, and J. A. Stroscio, Phys. Rev. Lett. **110**, 117001 (2013).
[16] T. Proslier, A. Kohen, Y. Noat, T. Cren, D. Roditchev, and W. Sacks, Europhys. Lett. **73**, 962 (2006).
[17] N. Bergeal, Y. Noat, T. Cren, T. Proslier, V. Dubost, F. Debontridder, A. Zimmers, D. Roditchev, W. Sacks, and J. Marcus, Phys. Rev. B **78**, 140507 (2008).
[18] H. Kimura, R. P. Barber, S. Ono, Y. Ando, and R. C. Dynes, Phys. Rev. B **80**, 144506 (2009).
[19] M. H. Hamidian, S. D. Edkins, S. H. Joo, A. Kostin, H. Eisaki, S. Uchida, M. J. Lawler, E.-A. Kim, A. P. Mackenzie, K. Fujita, J. Lee, and J. C. S. Davis, Nature, **532**, 343 (2016).
[20] M. E. Flatté and J. M. Byers, Phys. Rev. Lett. **78**, 3761 (1997).
[21] M. E. Flatté and J. M. Byers, Phys. Rev. B **56**, 11213 (1997).
[22] S. Misra, B. B. Zhou, I. K. Drozdov, J. Seo, L. Urban, A. Gyenis, S. C. J. Kingsley, H. Jones, and A. Yazdani, Rev. Sci. Instrum. **84**, 103903 (2013).
[23] P. Townsend and J. Sutton, Phys. Rev. **128**, 591 (1962).
[24] B. L. Blackford and R. H. March, Phys. Rev. **186**, 397 (1969).
[25] M. Ruby, B. W. Heinrich, J. I. Pascual, and K. J. Franke, Phys. Rev. Lett. **114**, 157001 (2015).
[26] M. Ternes, W.-D. Schneider, J.-C. Cuevas, C. P. Lutz, C. F. Hirjibehedin, and A. J. Heinrich, Phys. Rev. B **74**, 132501 (2006).
[27] G.-L. Ingold, H. Grabert, and U. Eberhardt, Phys. Rev. B **50**, 395 (1994).
[28] B. Jaeck, M. Eltschka, M. Assig, A. Hardock, M. Etzkorn, C. R. Ast, and K. Kern, Appl. Phys. Lett. **106**, 013109 (2015).
[29] A. Roychowdhury, M. Dreyer, J. R. Anderson, C. J. Lobb, and F. C. Wellstood, Phys. Rev. Appl. **4**, 034011 (2015).
[30] G.-L. Ingold and H. Grabert, Europhys. Lett. **14**, 371 (1991).
[31] See Supplemental Material at http://link.aps.org/supplemental/10.1103/PhysRevB.93.161115 for details of the fitting procedure as well as additional data and further discussion of Josephson and Andreev processes over the adatoms.
[32] B. Jäck, M. Eltschka, M. Assig, M. Etzkorn, C. R. Ast, and K. Kern, Phys. Rev. B **93**, 020504 (2016).
[33] V. Ambegaokar and A. Baratoff, Phys. Rev. Lett. **10**, 486 (1963).
[34] P. Anderson, J. Phys. Chem. Solids **11**, 26 (1959).
[35] A. A. Abrikosov and L. P. Gor'kov, Zh. Eksp. Teor. Fiz. **39**, 1781 (1960) [Sov. Phys. JETP **12**, 1243 (1961)].
[36] H. Shiba, Prog. Theor. Phys. **40**, 435 (1968).
[37] L. Yu, Acta Phys. Sin. **21**, 75 (1965).
[38] A. I. Rusinov, Sov. Phys. JETP **9**, 85 (1969).
[39] A. Yazdani, B. A. Jones, C. P. Lutz, M. F. Crommie, and D. M. Eigler, Science **275**, 1767 (1997).
[40] S.-H. Ji, T. Zhang, Y.-S. Fu, X. Chen, X.-C. Ma, J. Li, W.-H. Duan, J.-F. Jia, and Q.-K. Xue, Phys. Rev. Lett. **100**, 226801 (2008).
[41] G. C. Menard, S. Guissart, C. Brun, S. Pons, V. S. Stolyarov, F. Debontridder, M. V. Leclerc, E. Janod, L. Cario, D. Roditchev, P. Simon, and T. Cren, Nat. Phys. **11**, 1013 (2015).
[42] J. Heinrichs, Phys. Rev. **168**, 451 (1968).
[43] P. Schlottmann, Phys. Rev. B **13**, 1 (1976).
[44] M. Ruby, F. Pientka, Y. Peng, F. von Oppen, B. W. Heinrich, and K. J. Franke, Phys. Rev. Lett. **115**, 087001 (2015).